

CHAPTER 24

# *Using Microfluidics, Real-time Imaging and Mathematical Modelling to study GPCR Signalling*

ANDREJA JOVIC,<sup>a</sup> SHUICHI TAKAYAMA<sup>ab</sup> AND JENNIFER J. LINDERMAN<sup>\*c</sup>

<sup>a</sup> Biomedical Engineering Department, University of Michigan, Ann Arbor, MI, USA; <sup>b</sup> Macromolecular and Materials Science Engineering, University of Michigan, Ann Arbor, MI, USA; <sup>c</sup> Department of Chemical Engineering, University of Michigan, Ann Arbor, MI, USA

## **24.1 Introduction**

The combination of experimental and computational methods provides a powerful approach for understanding biological processes. Initial experiments can suggest hypotheses that can be captured by first-generation mathematical/computational models (henceforth simply called ‘mathematical models’ or ‘models’), which can then be employed to generate new experimental approaches to test those models. Understanding signal transduction pathways, with their myriad of molecular interactions, feedback loops, and spatial and temporal variations in concentrations of key molecules, requires such an iterative process between experiments and modeling.<sup>1</sup>

---

RSC Drug Discovery Series No. 8

G Protein-Coupled Receptors: From Structure to Function

Edited by Jesús Giraldo and Jean-Philippe Pin

© Royal Society of Chemistry 2011

Published by the Royal Society of Chemistry, [www.rsc.org](http://www.rsc.org)

Models of signal transduction pathways that are mechanistic (reflecting actual physical processes that occur as opposed to empirical or statistical models) typically have many parameters. The concentrations of various molecules along the pathways, the forward and reverse rate constants for binding reactions, diffusivities of key molecules, and enzymatic activities are all physical parameters that can appear in such models.<sup>2-5</sup> Yet values for all of these parameters are not known with certainty. Assays can of course be developed to measure some of the parameters. Yet how well those values translate from the assay conditions (often *in vitro*) to the cellular environment during signalling is typically not known.

This uncertainty in parameter values, combined with uncertainty in experimental measurements, can make the comparison between model and experiment difficult: does, for example, a 30% difference between the two reflect an incorrect parameter value, a small error in the experimental measurement, or a poor understanding of the governing physical processes when the model was formulated? One approach that is helpful is to develop *qualitative* tests for the comparison. In other words, although the output of both the model and the experiment are quantitative (*e.g.* numbers of G proteins activated or concentration of intracellular free calcium), a comparison of qualitative trends (*e.g.* does a curve rise or fall, or shift right or left) may be most useful, at least in the initial stages of understanding a mechanism. Thus, it is helpful to develop new (and multiple) qualitative tests that can be used for the comparison between proposed mechanisms (as formulated in a model) and experimental data.

In this chapter, we focus on G protein signalling, in particular G protein-coupled receptor (GPCR) mediated calcium oscillations. Numerous models have been developed to describe these calcium oscillations.<sup>6-12</sup> Here we describe a novel approach, the modelling and experimental analysis of phase-locking, which provides a qualitative test that can be used to evaluate those models.

Phase-locking analysis involves application of periodic stimulation to an oscillatory pathway, which then becomes synchronized to the stimulation inputs. While the phenomenon of phase-locking is intrinsic to all non-linear oscillators,<sup>13</sup> phase-locking behaviour may be different for different oscillatory mechanisms.<sup>14</sup> We first describe proposed mechanisms for GPCR-induced calcium oscillations, and then introduce simulation and experimental methods to analyse phase-locking properties of the oscillations. Finally, we demonstrate phase-locking analysis as applied to a GPCR-mediated calcium signalling pathway to elucidate signalling mechanisms.

## 24.2 Models of GPCR-induced Calcium Signalling

Mathematical modelling of GPCR-initiated signal transduction pathways, like all modelling of biological processes, offers the opportunity for us to interpret data, analyse hypothesized mechanisms, run virtual (*in silico*) experiments and motivate new experiments. For example, different pathways or physical mechanisms may be suggested to explain the same biological data. Designing

and performing experiments based on mathematical models that have been formulated for the proposed mechanisms can help distinguish between these mechanisms.

GPCR-induced intracellular calcium signalling has been the focus of many modelling studies, due in part to the discovery of calcium oscillations upon chemical stimulation of cells.<sup>15–17</sup> Another key observation was that increasing or decreasing the ligand concentration changes primarily the frequency and not the amplitude of calcium oscillations,<sup>8</sup> suggesting that critical information for signalling pathways is encoded in the frequency of calcium signals. These observations, along with estimation of some relevant kinetic parameters, led to the development of a variety of oscillatory calcium models whose mechanisms differ, often significantly, in terms of how oscillations are generated and calcium levels are set.<sup>6–12</sup> Most of these models are composed of ordinary differential equations based on mass action kinetics and assumptions of Michaelis–Menten kinetics, cooperativity (*e.g.* Hill coefficient), and similar. Upon solving these equations, one can track the dynamics of each of the cellular components [*e.g.* bound receptors, activated G proteins, inositol 1,4,5-trisphosphate (IP3) and intracellular free calcium concentration] over time.

For this chapter, we focus on two representative mathematical models of calcium oscillations with differing activation and recovery properties—one described by Chay *et al.*<sup>7</sup> and another by Politi *et al.*<sup>11</sup> (Figure 24.1). For the Chay *et al.* model (Figure 24.1 top left), calcium oscillations are produced by the switch-like (Hill coefficient of 4) activation of phospholipase C (PLC) by G proteins, which in turn produces IP3 and diacylglycerol (DAG). IP3 binds to IP3 receptors, opening calcium channels on intracellular stores and thus eliciting a calcium response. DAG initiates a negative feedback that subsequently reduces G protein activity, resulting in calcium oscillations. A basal level of G protein activity that results in basal IP3 production is included, ensuring that IP3 levels return to pre-stimulus levels. In this model, signalling is initiated by increasing the receptor contribution to the rate of G protein activation, indicated by the term ‘stimulant’ in Figure 24.1.

In contrast, the Politi *et al.* model (Figure 24.1 top right) assumes that activation of PLC by G proteins is a graded process (as opposed to switch-like). In other words, the rate of PLC activation is proportional to the number of activated G proteins. Production of IP3 initiates a feedback loop between the IP3 receptor (IP3R), calcium and PLC that leads to calcium oscillations. Furthermore, the model does not include a mechanism for basal IP3 production, highlighting a difference in recovery properties of the respective models in addition to the difference in their activation properties. In the Politi *et al.* model, signalling is initiated by increasing the rate at which phosphatidylinositol 4,5-bisphosphate (PIP2) is converted to IP3 (by activated PLC). Parameters for both models were derived from a combination of experimental data and estimation.

Despite having different mechanisms for generating calcium oscillations, the two models behave nearly identically when addressed with continuous stimulation; both models produce calcium oscillations upon application of continuous stimulation. The period of these oscillations decreases with increasing

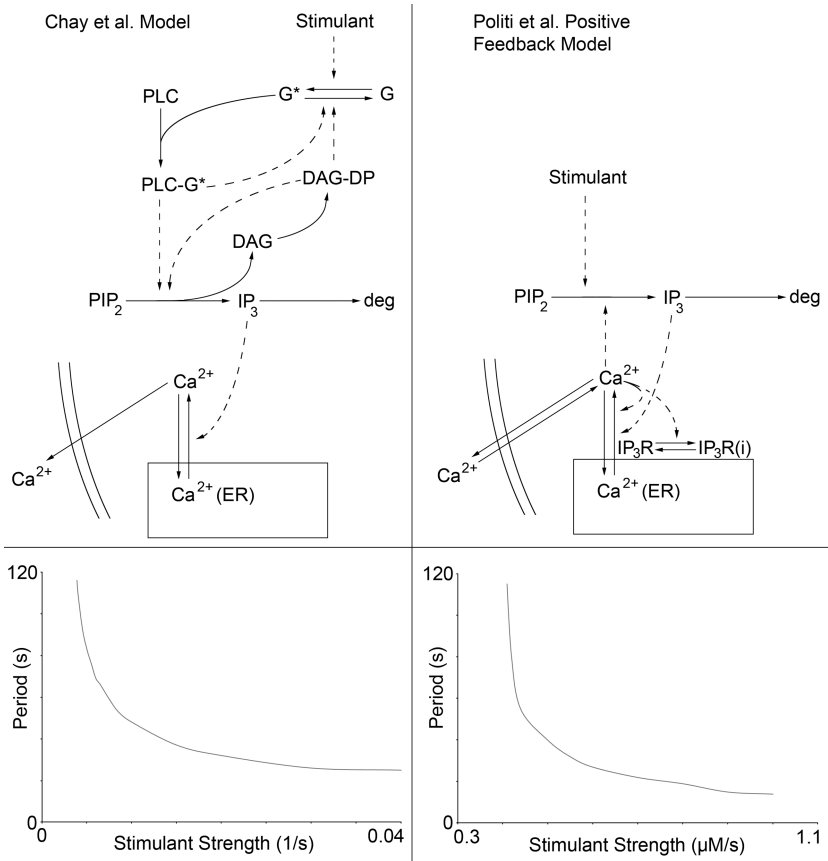


**Figure 24.1** Schematics of the two mathematical models of oscillatory calcium signalling analysed in this chapter: the Chay *et al.* model<sup>7</sup> (top left) and the positive feedback Politi *et al.* model<sup>11</sup> (top right). Original published equations and parameters were used for both models. Under continuous stimulation, both models produce calcium oscillations whose period decreases with increases in stimulant strength (bottom figures). Despite significant differences in the mechanisms between these models, they exhibit the same behaviours under continuous stimulation. The stimulant strengths have different units, based upon the molecular species in the models that convey information about stimulant strength. For the Chay *et al.* model, the molecular species is the active agonist/receptor complex; for the Politi *et al.* model, the molecular species is the PLC/activated G-protein complex (PLC-G\*). G = G protein; G\* = activated G protein; PLC = phospholipase C; PIP<sub>2</sub> = phosphatidylinositol 4,5-bisphosphate; IP<sub>3</sub> = inositol 1,4,5-trisphosphate; DAG = diacylglycerol; DAG-DP = DAG dependent protein; deg = degradation; Ca<sup>2+</sup> = calcium; ER = endoplasmic reticulum; IP<sub>3</sub>R = IP<sub>3</sub> receptor; IP<sub>3</sub>R(i) = inactive IP<sub>3</sub>R.

stimulation strength (Figure 24.1 bottom left and 24.1 bottom right), demonstrating that this widely applied qualitative test is insufficient to distinguish between these (and many other) model mechanisms.

These and other results demonstrate that analysis of calcium transients elicited with continuous stimulation (*e.g.* the oscillations shown here) or simple step changes in stimulation (*e.g.* a sudden increase in ligand concentration) are insufficient to adequately probe the calcium signalling pathway. Are there additional tests available to distinguish between proposed model mechanisms for GPCR-induced calcium oscillations? As described below, phase-locking behaviour may provide one such test.

### 24.3 Phase-locking and Sub-threshold Calcium Responses

Phase-locking refers to the phenomenon whereby an oscillatory system synchronizes to a periodic input (Figure 24.2). Phase-locking is predicted to occur for all non-linear oscillators;<sup>13</sup> for example, it was explored in oscillatory electrical systems exposed to periodic electrical stimulation for the purpose of understanding how to better control such non-linear systems.<sup>18</sup> In a biological context, phase-locking has been observed in experiments with cardiac<sup>19</sup> and neuronal systems.<sup>20</sup> In these studies, periodic electrical stimulation was supplied and the corresponding cellular (electric) responses were measured.

Several studies have indicated that the simple observation of phase-locking alone does not provide insight into the mechanisms of oscillatory systems.<sup>13</sup> However, phase-locking properties (*e.g.* how phase-locking changes, or not, with different stimulation parameters) can provide insight into oscillatory mechanisms. Seminal studies of phase-locking in cardiac cell aggregates found that as the rest period between periodic electrical stimulation events was reduced, the cells' capacity to keep up with the stimulatory inputs was also reduced.<sup>19</sup> In other words, the number of cellular responses was less than the number of stimulation events, indicative of skipped beats. To quantify the cells' capacity to keep up with periodic stimulation, one can use the metric called the phase-locking ratio (PLR), elsewhere referred to as the Winding number (Figure 24.2). One can define the phase locking ratio PLR as:

$$\text{PLR} = \frac{\text{number of system responses}}{\text{number of stimulation events}} \quad (24.1)$$

Theoretical studies have characterized the effects of periodic stimulation parameters on the PLR.<sup>7</sup> Periodic stimulation parameters include the stimulant concentration (C), the stimulation duration (D) and the rest period (R) (Figure 24.3). When the PLR is plotted against the value of a single periodic stimulation parameter (while holding the others constant), what has been termed a 'Devil's Staircase'<sup>7</sup> emerges (Figure 24.3).

Examining how the PLR changes with simulation parameters gives insight into activation and recovery properties of the oscillatory system. Depending upon the activation and recovery properties of the system, the staircase may increase or decrease; in other words, the PLR may increase or decrease with increasing C, D or R, based upon the activation and recovery properties of the

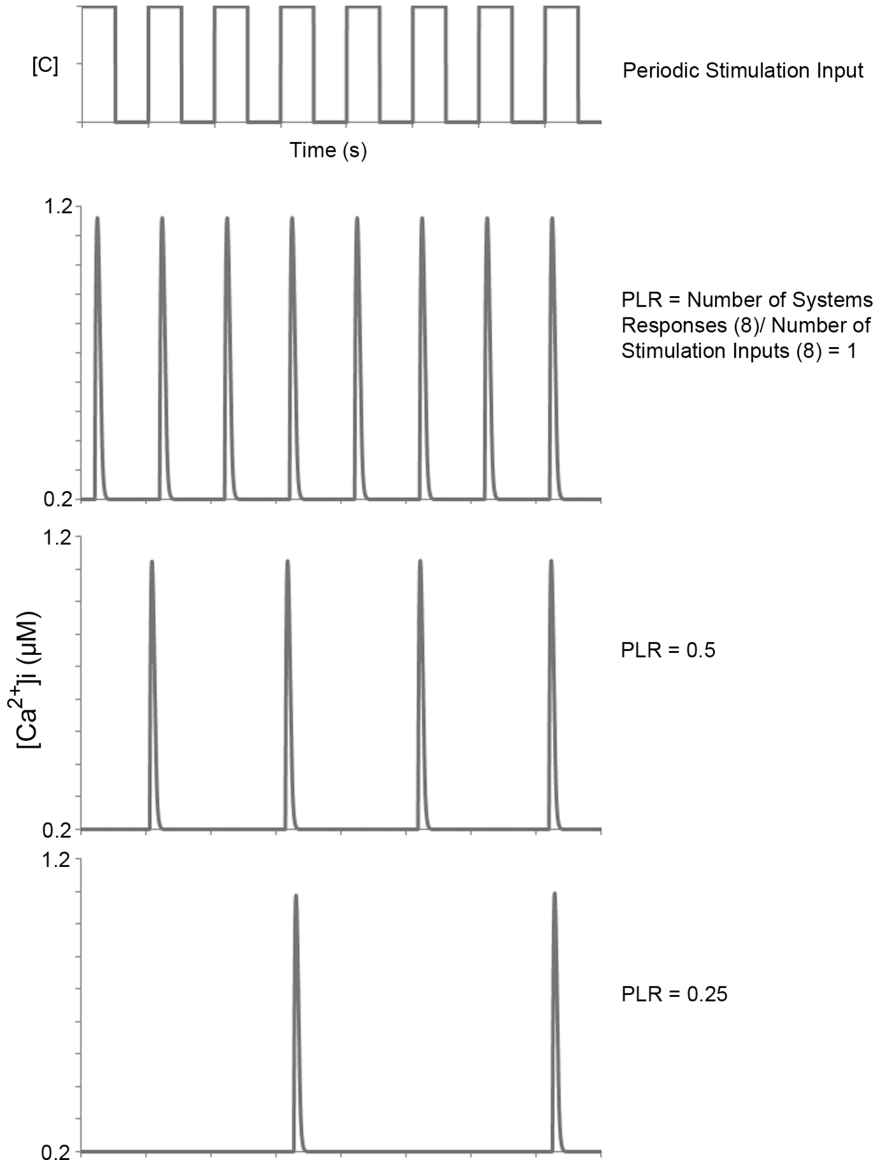


**Figure 24.2** Phase-locking of calcium responses to a periodic stimulation input and calculation of the phase-locking ratio (PLR). Top trace shows the periodic stimulation input applied to a single cell, here a pulse of agonist with concentration  $[C]$ . For the three calcium traces depicted, the calcium responses are synchronized to the periodic stimulation input. A calcium response only results during a stimulation event; however, not every stimulation event necessarily elicits a calcium response, indicative of a loss of fidelity. To assess the degree of fidelity, the PLR is calculated by dividing the number of system responses by the number of stimulation events.

oscillatory system. In our experience with calcium oscillation models, increasing  $C$  or  $D$  typically results in an increase in the PLR, since both parameters increase the chances that a system response will occur. Thus, modifying these two stimulation parameters may not provide the insight needed to discriminate between various proposed oscillation mechanisms.

However, with calcium oscillation models, we find that when the PLR is plotted against the rest period  $R$ , the Devil's Staircase plot that results reveals recovery properties of the oscillatory system. Do cellular levels of key molecules (IP3, calcium) slowly or rapidly return to baseline values or perhaps overshoot baseline values and spend some time at reduced levels? These features affect the ability of the system to respond to the next stimulation pulse. Thus, periodic stimulation can provide insight into the recovery properties, a feat difficult to attain with continuous stimulation and conventional experimental techniques.

In calculating PLR, it is typical to count only 'full' responses; researchers have also observed 'sub-threshold' responses upon exposure of oscillatory systems to periodic stimulation<sup>21</sup> (Figure 24.3). Here 'sub-threshold' delineates that a system response did not reach full amplitude. This type of response represents a unique activation property that emerges only from periodic stimulation, and it may also be useful in comparing mechanisms.

## 24.4 Phase-locking Analysis of GPCR-induced Calcium Signalling in Two Models

Proposed GPCR-induced calcium oscillation models can be examined for the existence and properties of phase-locking.<sup>14</sup> Periodic stimulation in the form of ligand pulses can be used as a model input, and analysis proceeds as described in Figure 24.3. Here we focus on the Chay *et al.* and Politi *et al.* models. Because neither model explicitly includes receptor/ligand binding, periodic stimulation is implemented by periodic increases in the receptor contribution to the rate of G protein activation (Chay *et al.* model) or periodic increases in the rate at which PIP2 is converted to IP3 (Politi *et al.* model). We have also explicitly added the equations describing receptor/ligand/G protein dynamics to these models, and the phase-locking behaviour is similar to that shown here.<sup>14</sup> Phase-locking of the calcium responses is observed with both models, as expected for any non-linear oscillator<sup>13</sup> (Figure 24.4A). Under some periodic stimulation conditions, the calculated PLR for both models is less than one (Figure 24.4), indicative of skipped beats and consistent with observations in other experimental<sup>19</sup> and theoretical systems.<sup>7</sup> Note that the Politi *et al.* model, but not the Chay *et al.* model, shows sub-threshold calcium responses (Figure 24.4A). This result demonstrates that the activation properties of the two mathematical models are different, despite the similarity in signalling behaviour upon continuous stimulation seen in Figure 24.1.

To assess the phase-locking behaviours of the two models, each was exposed to periodic stimulation while the stimulant concentration ( $C$ ), stimulation duration ( $D$ ) or rest period ( $R$ ) was varied. As seen in Figure 24.4B and 24.4C,

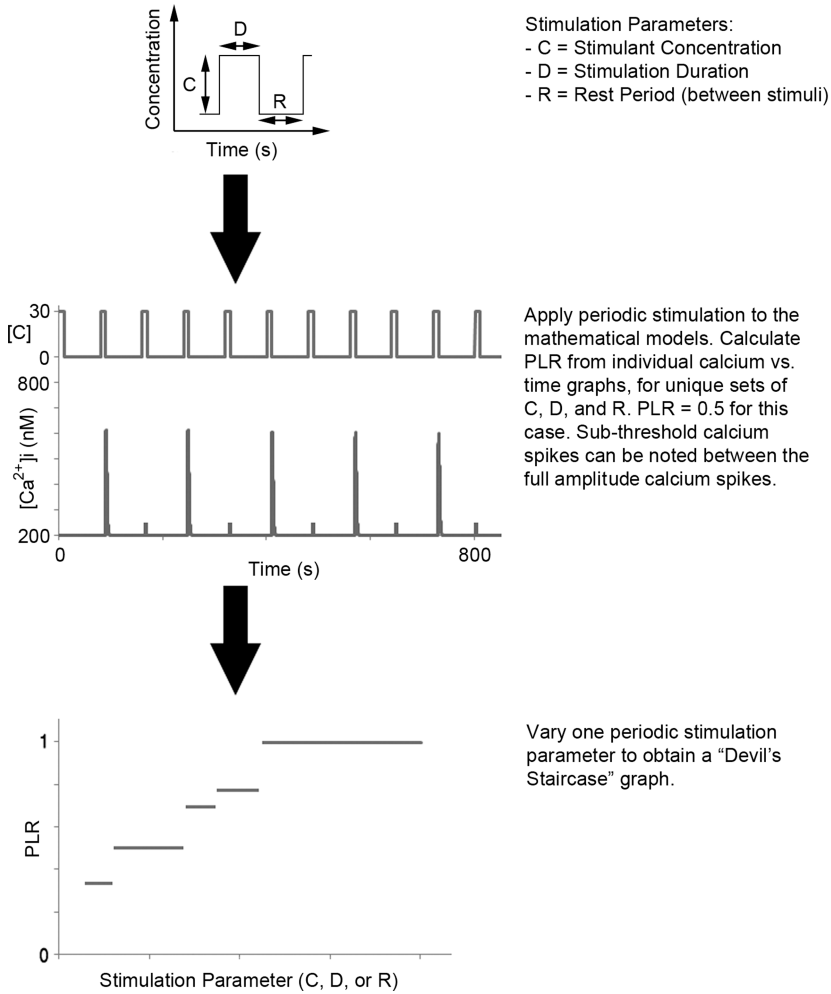


**Figure 24.3** Procedure for assessing the effect of stimulation parameters on the phase-locking ratio (PLR) in mathematical models, to develop a set of discriminating markers for comparison to experiments. Periodic stimulation is applied to a single cell described by one of the mathematical models and the PLR is calculated. A single stimulation parameter (C, D or R) is varied and the PLR is calculated for every value. Plotting PLR vs. the stimulation parameter value results in a 'Devil's Staircase' graph. The relationship between the stimulation parameter and the PLR (increasing or decreasing) provides a discriminating feature for comparison to experiments.

the behaviour of both models when only C or D was varied is similar. However, plotting the phase-locking ratio against the rest period provides a discriminating marker: PLR increases as the rest period increases for the Chay *et al.* model, while the opposite trend occurs for the Politi *et al.* model

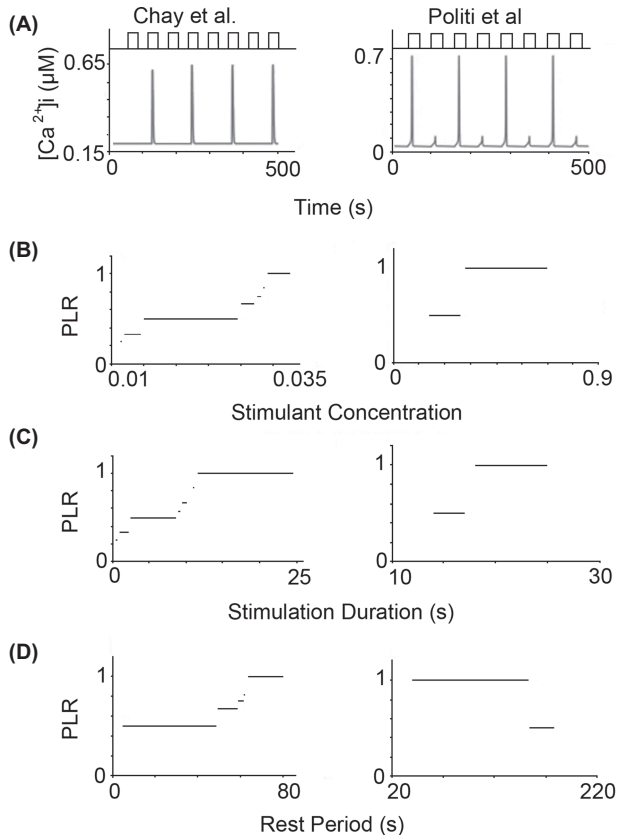


**Figure 24.4** Unique signalling properties uncovered by phase-locking analysis of the Chay *et al.* and Politi *et al.* mathematical models. Original published equations and parameters were used for both models. (A) Periodic stimulation of the Chay *et al.* model leads to skipped beats with the absence of sub-threshold spikes. Periodic stimulation of the Politi *et al.* model also leads to skipped beats, but features sub-threshold spikes. (Chay *et al.* model:  $C = 0.03$  1/s; Politi *et al.* model:  $C = 0.8$  µM/s. For both:  $D = 30$  s,  $R = 30$  s). (B) PLR vs.  $C$  (Chay *et al.* model:  $D = 10$  s,  $R = 50$  s; Politi *et al.* model:  $D = 10$  s,  $R = 50$  s). (C) PLR vs.  $D$  (Chay *et al.* model:  $C = 0.03$  1/s,  $R = 60$  s; Politi *et al.* model:  $C = 0.8$  iM/s,  $R = 60$  s). (D) PLR vs.  $R$  (Chay *et al.* model:  $C = 0.03$  1/s,  $D = 10$  s; Politi *et al.* model:  $C = 0.8$  µM/s  $D = 10$  s).

(Figure 24.4D). This difference suggests a difference in recovery properties for the two models. Importantly, note that the models can be easily distinguished *via* a qualitative comparison, *i.e.* one model predicts an increase in PLR with  $R$  and the other predicts a decrease, and that this behaviour should be readily apparent in experimental data.

Investigation of the respective model architectures reveals the mechanisms responsible for the differing activation and recovery properties. We can first

examine the activation behaviour. The Chay *et al.* model does not exhibit sub-threshold calcium responses because of a switch-like activation of PLC by G proteins; the Hill coefficient of the reaction is four in this model. In contrast, the Politi *et al.* model exhibits sub-threshold calcium responses because G protein-mediated activation of PLC is graded. In terms of recovery properties, the Chay *et al.* model contains a basal G protein activity that results in basal IP<sub>3</sub> production. Basal IP<sub>3</sub> production promotes recovery to resting levels between stimulation events, and thus with longer rest periods, IP<sub>3</sub> levels are higher and more likely to cross the threshold necessary to elicit a calcium response with a subsequent stimulation event. Ultimately, this results in an increase in PLR as R is increased. In contrast, the Politi *et al.* model has no such recovery mechanism; IP<sub>3</sub> levels subside as the rest period increases and so calcium responses are less likely to occur with a subsequent stimulation event. As a result, one observes a reduction in PLR as R is increased.

These model observations provide a concrete set of discriminating markers that can be compared with experimental results. However, typical experiments assessing GPCR-induced calcium oscillations rely on continuous stimulation or on a single step change increase in ligand concentration. Thus experimental setups that are able to stimulate cells periodically and allow for real-time imaging of the resulting intracellular calcium responses must be developed.

## 24.5 Microfluidics to Enable Pulsatile Stimulation of Cells

The ability to carry out phase-locking analysis for the study of G protein dynamics is dependent upon the ability to reproducibly control cellular stimulation with high temporal resolution. Conventional techniques for creating dynamic cellular stimulation conditions are deficient in this respect; these methods typically involve adding known amounts of ligand to cells growing in culture dishes or on glass slides, effectively exposing cells only to step increases in stimulant concentration.<sup>22</sup> This approach is not amenable to the generation of reproducible periodic stimulation patterns necessary to study phase-locking. For example, it is difficult to exchange fluid rapidly because it requires a user to manually address cells repeatedly with stimulant, aspirate the stimulant away, and then reapply the stimulant, within a matter of tens of seconds. Perfusion chambers represent an advance in terms of reproducibility, but these setups lack versatility and scalability.<sup>23</sup>

The advent of microfluidic technology has overcome many of these limitations (Figure 24.5A). In terms of scalability, entire biochemical and genetic operations and manipulations are executed on a platform several square inches in area. The crux of this technology is the ability to harness the physical properties of liquids on the micron scale, enabling enhanced control over spatial and temporal facets of cellular stimulation, and thus versatility. While microfluidics initially garnered interest for studies of spatial dynamics,<sup>24,25</sup> recently it has become increasingly utilized for studies of temporal dynamics of

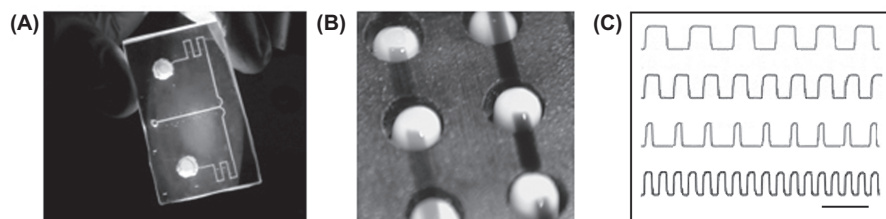


**Figure 24.5** The microfluidic setup is able to control three stimulation parameters (C, D and R) (see Figure 24.3). (A) Image of the microfluidic setup filled with fluorescein solution. (B) Braille-actuated pumping controls fluid flow through channels. (C) Pulses generated by the microfluidic setup are reproducible and high temporal resolution is achievable. (Scale bar = 90 s).

cell signaling.<sup>26</sup> The appeal of this method is the rapid fluid exchange that can be achieved, as well as the low reagent consumption, portability and potential for high throughput analysis. For example, Hersen *et al.*<sup>27</sup> developed a microfluidic device capable of addressing cells with a chemical stimulant at frequencies  $\leq 2$  Hz without disrupting cell adhesion. G protein signalling occurs on the sub-second to seconds time scale, while G-protein-mediated calcium signalling is generally on the order of tens of seconds to minutes. Thus, microfluidic technology provides an optimal platform for investigations of these dynamics.

The ability to rapidly customize experimental setups for study of the dynamics of a particular GPCR ligand-receptor in a specific cell type is another major advantage of microfluidics over conventional techniques. Microfluidic devices can be designed and fabricated in  $\sim 24$  hours. Most microfluidic devices are created by a rapid prototyping method pioneered by the Whitesides group.<sup>28</sup> Initially, microfluidic designs are created on a computer aided design (CAD) program and these designs are then converted into a transparency. The transparency design is transferred to a silicon wafer or glass slide through a photolithographic process, effectively creating a mould with positive relief features. The overwhelming choice of material for creating microfluidic devices is polydimethylsiloxane (PDMS); this silicon-based elastomer has favourable properties for cell culture and imaging.<sup>29</sup> PDMS is cast against the mould, and upon curing, the device is irreversibly sealed against a flat surface (usually glass or PDMS sheet) through plasma oxidation. Microfluidic devices can be customized for a particular cell type in a number of ways; for instance, for cell types that do not adhere well to PDMS or glass surfaces, the device surface can be coated with adhesion molecules such as laminin or fibronectin.<sup>30</sup> More elaborate manipulations can be implemented to support culture of cells that are difficult to grow *in vitro*.<sup>31</sup>

The method for pumping liquid in the microfluidic devices plays a tremendous role in the design and fabrication process. The most common pumping methods employed in microfluidics are gravity-driven and syringe-mediated pumping, of which the latter is more reliable. More elaborate pumping systems include 'Quake valves',<sup>32</sup> Braille actuation,<sup>33,34</sup> acoustics,<sup>35</sup> and most recently autonomous pumping regulation by embedded components.<sup>36</sup>

The reproducibility and versatility of generation of temporal patterns is in large part determined by the pumping mechanisms implemented for conveying fluids through the microfluidic channels. In our experiments, we use Braille-actuated pumping, which offers an excellent level of control, reproducibility and portability<sup>33,34</sup> (Figure 24.5B). With this approach, microfluidic channels are aligned on a Braille display that is connected to a computer *via* USB. Upon elevation, individual Braille pins are able to valve off the microfluidic channels that lie above, due to the elastomeric nature of the PDMS. In the appropriate sequence, consecutive Braille pin movements enable relatively unidirectional flow. Individual Braille pin movements are controlled by a computer program, such that the speed and direction of pumping can be regulated. This setup provides an optimal platform for conducting studies in which control over cellular stimulation parameters, such as stimulation duration and rest between stimulation events, is required. This is demonstrated in Figure 24.5C; one reservoir of the device was filled with fluorescein solution and the other with water. Upon alternating from which reservoir liquid was pumped, square-wave patterns of specific duration and rest period were reliably generated.<sup>37</sup>

## 24.6 Imaging of Signalling Dynamics in a Microfluidic Device

In order to monitor cellular signalling dynamics resulting from temporal patterns of stimulation, real-time imaging of appropriate readouts of cell signalling is needed. The advent of fluorescent reporters of cell signalling has enabled tracking of signalling behaviours of individual cells. In particular, green fluorescent protein (GFP) based readouts (or variants of GFP) have been employed to track the localization, translocation, appearance or degradation of intracellular components, representing ‘passive’ applications of these fluorescent constructs; in this context, ‘passive’ denotes that the component activity is not assessed.

Fluorescence resonance energy transfer (FRET) has been used in order to convey dynamic information about intracellular activity.<sup>38</sup> Although FRET probes for directly assessing G protein activity have been developed,<sup>39</sup> the dynamic range of these readouts has not reached a level that has led to widespread utilization. However, the following are some of the probes developed over the last 15 years that are able to track G protein-mediated signalling activities: Cameleon (for intracellular calcium);<sup>40</sup> Raichu-Ras (measures levels of activated Ras);<sup>41</sup> cGMP probe;<sup>42</sup> PKA probe; and a cAMP probe.<sup>43</sup>

In this chapter, the focus is on using G protein-mediated calcium signalling to elucidate molecular mechanisms. Since imaging probes for calcium are more developed compared with those for G proteins,<sup>39</sup> intracellular calcium is used as a readout to infer G protein signalling dynamics. While the fluorescent

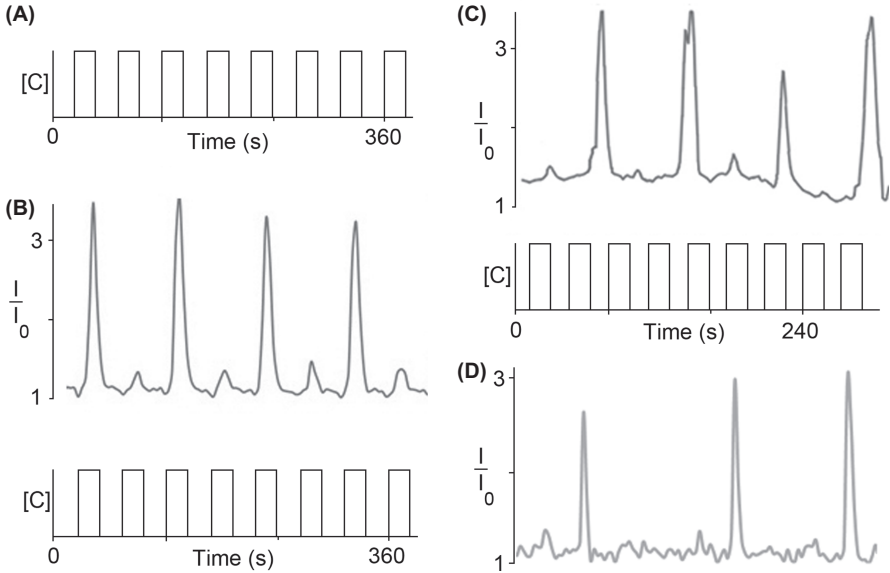
protein aequorin<sup>44</sup> has been utilized for assessing intracellular calcium levels in real-time, it is labour-intensive to introduce into cells, requiring micro-injection. Since high throughput analysis of cells is thus not feasible with this indicator, fluorescent dyes and genetically coded probes are preferred. Fura-2 and Fluo-4 are popular fluorescent dyes;<sup>45,46</sup> these probes can be easily introduced into cells and are commercially available. These dyes can leak out, rendering them infeasible for use in long-term experiments and it has been reported that the dyes can localize to various compartments of cells, complicating quantification of calcium levels. Genetically encoded FRET probes for calcium can be easily introduced into cell populations through transfection.<sup>47</sup> In addition, these probes are specifically designed to localize to a specific part of the cell and do not leak out, enabling long-term characterizations of calcium dynamics. For these reasons, we used the FRET probe YC3.60 developed by Nagai *et al.*,<sup>48</sup> which measures free calcium levels exclusively in the cytosol.

## 24.7 Experimental Observations of Phase-locking in GPCR-induced Calcium Signalling

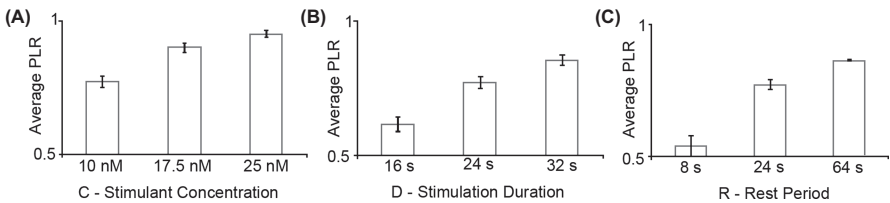
Using the microfluidic and imaging techniques described above, one can measure GPCR-induced calcium oscillations and compare those data with the phase-locking properties of models to elucidate mechanisms. Using our Braille-actuated microfluidic platform, cells were periodically exposed to ligand and the resulting calcium signals were recorded in real-time using the FRET probe YC3.60.<sup>14</sup> The D and R values chosen for these studies were based upon the typical durations of single oscillatory calcium responses (tens of seconds) and typical oscillation periods (tens of seconds to minutes).

Figure 24.6 shows the calcium responses of three cell types exposed to periodic stimulation with different GPCR ligands: a HEK293 cell stimulated with carbachol (through the M3 receptor); a HeLa cell stimulated with histamine (through histamine receptors); and a HeyA8 cell stimulated with extracellular calcium (through the calcium-sensing receptor), respectively. Phase-locking was observed with each cell type, as calcium responses were synchronized to the periodic stimulation events. Furthermore, all three cells exhibited PLRs less than one, as predicted by the models under some periodic stimulation conditions. Thus phase-locking is a general result of periodic stimulation of GPCR systems and phase-locking analysis may be appropriate to analyse signalling mechanisms.

For the remainder of this chapter, we focus our phase-locking analysis on the M3 muscarinic pathway in HEK293 cells in order to elucidate mechanisms of G protein (here, Gq) signalling. Periodic stimulation of HEK293 cells with carbachol resulted in phase-locking of the resulting calcium responses and sub-threshold spikes are present (Figure 24.6B). We then examined the phase-locking ratio as stimulant concentration (C), stimulation duration (D) or rest period (R) was varied. The PLR was measured for individual cells and then averaged. The population-averaged PLR can be used to compare between



**Figure 24.6** Observation of phase-locked calcium responses and sub-threshold spikes in three different cell types and with three different agonists. (A) Periodic stimulation pattern. (B) HEK293 cell periodically stimulated with carbachol ( $C = 10$  nM,  $D = 24$  s,  $R = 24$  s). (C) HeLa cell periodically stimulated with histamine ( $C = 100$   $\mu$ M,  $D = 24$  s,  $R = 24$  s). (D) HeyA8 cell periodically stimulated with extracellular calcium ( $C = 2$  mM,  $D = 16$  s,  $R = 16$  s). Here  $I/I_0$  signifies the FRET ratio of the calcium signal ( $I$ ) normalized to the minimum FRET ratio ( $I_0$ ), as has been done previously for analysis of intracellular calcium responses.<sup>48</sup>



**Figure 24.7** Experimentally measured average phase-locking ratios of cell populations vs. increasing  $C$ ,  $D$ , or  $R$  in HEK293 cells periodically stimulated with carbachol. (A) PLR vs.  $C$  ( $D = 24$  s,  $R = 24$  s). (B) PLR vs.  $D$  ( $C = 10$  nM,  $R = 24$  s). (C) PLR vs.  $R$  ( $C = 10$  nM,  $D = 24$  s). As each stimulation parameter was increased, there was a corresponding increase in the PLR, providing useful comparisons to mathematical model predictions. The results presented here are representative of at least 60 cells at each condition from three different experiments.<sup>14</sup>

different experimental conditions (Figure 24.7). Note that as  $C$  is increased, PLR increases; the same trend is observed when  $D$  is increased (Figure 24.7A and 24.7B). Thus increasing either  $C$  or  $D$  enhances the probability that a

calcium response is going to result during a particular stimulation event. We also found that increases in R produced increases in PLR (Figure 24.7C), suggesting that a recovery mechanism allows a reset of the signalling system if there is enough time between stimulation events.

## 24.8 Comparing Model and Experimental Results

These experiments described above (Figure 24.7) provide data on the M3 system for comparison with model predictions on phase-locking. The models introduced above and the experimental data show increases in PLR with C or D, so this comparison does not allow the models to be distinguished. However, because sub-threshold oscillations are not seen with the Chay *et al.* model, and because PLR decreases with R rather than increases with the Politi *et al.* model, neither mathematical model is able to account for all of our experimental observations even at a qualitative level.

A comparison between the models offers insights into GPCR-induced calcium oscillations mechanisms, particularly the activation and recovery properties of the M3 receptor/cell system are studied. The presence of sub-threshold calcium responses (Figure 24.6B) suggests that the G protein activation of PLC is graded and not switch-like as modelled by Chay *et al.* The G protein activation properties thus appear more similar to those of the Politi *et al.* model. However, increasing the rest period R in experiments resulted in increases in PLR (Figure 24.7C). This result indicated that the recovery properties of the system were better described by the Chay *et al.* model, suggesting the existence of basal G protein activity driving basal IP<sub>3</sub> production.

## 24.9 Model Revision

At least two approaches can be suggested to come up with a mechanistic model that is more consistent with the experimental data. First, we can learn from the comparison above and combine elements of each model to produce a model that does a better job of agreeing with the data. In order to undertake mechanism revision, elements from the respective calcium models that resulted in correct predictions of the activation and recovery properties of the system were combined.<sup>14</sup> Phase-locking analysis indicated that the Chay *et al.* model had the correct recovery properties, due to the inclusion of a basal G protein activity mechanism. Analysis also suggested that the Politi *et al.* model possessed the correct activation properties, due to the graded activation of PLC by G-proteins. Combining these two mechanistic elements, we created a revised model and then evaluated it using phase-locking analysis (Figure 24.8). Periodic stimulation resulted in the emergence of sub-threshold calcium responses, confirming an improvement in the activation properties of the new model (Figure 24.8A). As the rest period of the periodic stimulation increased, the phase-locking ratio correspondingly increased (Figure 24.8E), indicating that the recovery properties of the new system were accurate.

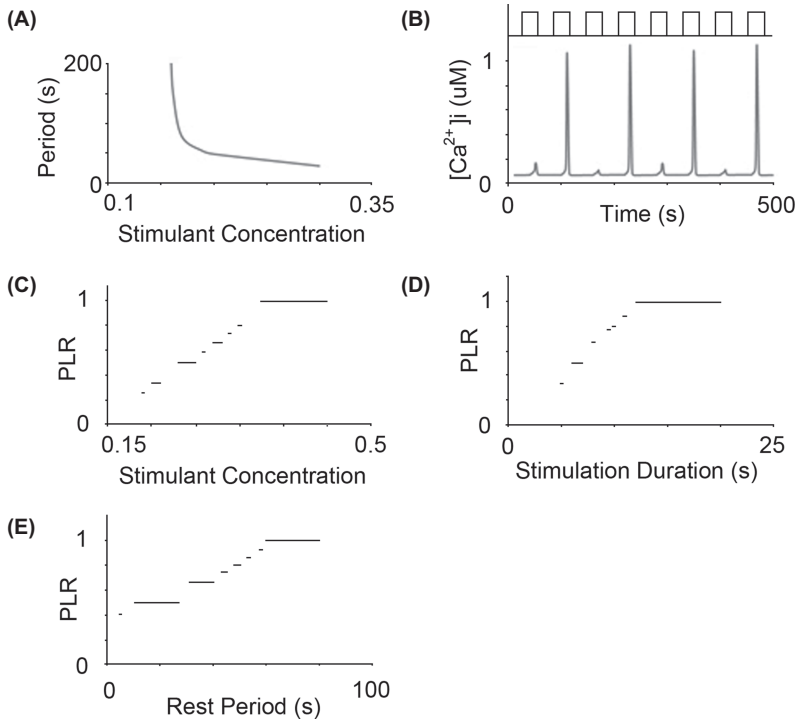


**Figure 24.8** Behaviours of the revised model (with basal IP<sub>3</sub> production = 0.3  $\mu\text{M/s}$ ) agree with experimental results of our phase-locking analysis. The model was revised by adding the basal IP<sub>3</sub> production term to the rate equation describing IP<sub>3</sub> production by PLC. (A) The revised model correctly predicts that under continuous stimulation, the calcium oscillation period decreases with increasing stimulant concentration ( $\mu\text{M/s}$ ). (B) The model correctly predicts the presence of sub-threshold calcium spikes upon periodic stimulation ( $C = 0.3 \mu\text{M/s}$ ,  $D = 10 \text{ s}$ ,  $R = 50 \text{ s}$ ). (C,D,E) Model predictions as stimulation concentration, stimulation duration, and rest period are varied: PLR vs.  $C$  ( $\mu\text{M/s}$ ) ( $D = 10 \text{ s}$ ,  $R = 50 \text{ s}$ ). PLR vs.  $D$  ( $C = 0.3 \mu\text{M/s}$ ,  $R = 50 \text{ s}$ ). PLR vs.  $R$  ( $C = 0.3 \mu\text{M/s}$ ,  $D = 10 \text{ s}$ ).

The second approach takes account of the fact that the discrepancies between models and experiments could be the result of incorrect parameter values in the model. Uncertainty in model parameter values is a given, as assays to measure all parameter values *in vivo* simply are not available. The Politi *et al.* model has 17 independent parameters, while the Chay *et al.* model has ten—most of which were estimated and not measured directly. Rather than haphazardly attempting to explore all possible parameter space, a sampling algorithm can be used to effectively search a large parameter space to explore whether the differences between the models and experiments are the result of the model parameter values but not mechanisms. Latin Hypercube Sampling (LHS) is an algorithm that we have implemented for this purpose; it entails specifying a distribution (e.g. normal or uniform) and dividing it up into equal probability intervals

from which to sample without replacement.<sup>4,49,50</sup> LHS is generally run for hundreds to thousands of iterations and allows for simultaneous variation of multiple model parameter values. In the context of this study, LHS was run for both the Chay *et al.* and Politi *et al.* models to observe whether any parameter set could result in the emergence of sub-threshold calcium responses. Parameters were sampled both from a normal distribution (with original parameters for the mean and with a standard deviation of 100%) and a uniform distribution (with a minimum of 0.1 times original parameter values and a maximum of ten times original parameter values). None of the parameter sets sampled were able to result in behaviour that agreed with our experimental results.

## 24.10 Future Directions

We have demonstrated in this chapter that phase-locking analysis can provide a useful tool for evaluating proposed mechanisms of GPCR-induced calcium oscillations. In particular, phase-locking can reveal aspects of the activation and recovery properties of oscillatory systems, particularly when the stimulation time and time between stimulation events are varied. Importantly, phase-locking analysis provides a qualitative tool: the ability of proposed models to reproduce experimental behaviour, *i.e.* the existence (or not) of sub-threshold oscillations and the behaviour (unchanged, increasing, decreasing) of the phase-locking ratio (PLR) as stimulation parameters are varied can be assessed. We demonstrated this concept here with two mathematical models of oscillatory calcium signalling (and with seven more models in ref. 14). As another qualitative test, Sneyd *et al.*<sup>51</sup> detailed an approach that involves subjecting cells to a pulse of IP<sub>3</sub> and observing whether subsequent calcium oscillations increase or decrease in frequency. This qualitative readout of GPCR signalling can help determine whether IP<sub>3</sub> oscillations are passive reflections of calcium oscillations or absolutely necessary to produce the calcium oscillations. A proposed mechanism that succeeds in passing qualitative tests can then be subjected to more quantitative tests and rigorous determination of physical parameter values. These tools complement existing genetic and chemical tools for deciphering GPCR signalling.

With advancements in imaging and synthesis, other probes should be available for phase-locking analysis and thereby provide even more discriminating markers for evaluation of mathematical models and elucidation of signalling pathways. Direct imaging of G protein dynamics has been achieved,<sup>39</sup> and with further development would be interesting to use for phase-locking analysis. Other relevant signalling components to image would be IP<sub>3</sub>,<sup>52</sup> and perhaps protein kinase C (PKC)<sup>53</sup> and the regulator of G protein signalling (RGS) proteins.<sup>54</sup>

Microfluidic technology will also allow other stimulation patterns to be tested. The phase-locking analysis described here relied on the ability to generate periodic (square-wave) stimulation. Other stimulation patterns such as

saw-tooth patterns,<sup>55</sup> different step patterns<sup>23,56</sup> and sine waves<sup>57</sup> are examples of stimulation patterns that could be used in this context and might expand the number of discriminating markers available for evaluating models and elucidating mechanisms.

Collectively, the combination of microfluidics, real-time imaging, and mathematical modelling provides a means of effectively elucidating molecular mechanisms of signalling that has many future possibilities.

## Acknowledgements

The authors would like to thank Bryan Howell, Michelle Cote, Susan M. Wade, Khamir Mehta, Atsushi Miyawaki and Richard R. Neubig for assistance with various aspects of the experimental or modelling work, and/or helpful comments.

This research was supported by the following sources: NIH Microfluidics in Biomedical Sciences Training Program (NIH NIBIB T32 EB005582), NIH ARRA Summer Supplement, NIH grants R01 HL084370-04, R01 CA136829-01, R33 HL092844, and the US Army Research Laboratories and the US Army Research Office (under contract number DAAD 19-03-1-0168).

## References

1. J. J. Linderman, *J. Biol. Chem.*, 2009, **284**, 5427–5431.
2. P. Bisegna, G. Caruso, D. Andreucci, L. Shen, W. Gurevich, H. E. Hamm and E. DiBenedetto, *Biophys. J.*, 2008, **94**, 3363–3383.
3. S. J. Bornheimer, M. R. Maurya, M. G. Farquhar and S. Subramaniam, *Proc. Natl. Acad. Sci. U. S. A.*, 2004, **101**, 15899–15904.
4. T. L. Kinzer-Ursem and J. J. Linderman, *PLoS Comput. Biol.*, 2007, **3**, 84–94.
5. J. J. Saucerman, J. Zhang, J. C. Martin, L. X. Peng, A. E. Stenbit, R. Y. Tsien and A. D. McCulloch, *Proc. Natl. Acad. Sci. U. S. A.*, 2006, **103**, 12923–12928.
6. A. Atri, J. Amundson, D. Clapham and J. Sneyd, *Biophys. J.*, 1993, **65**, 1727–1739.
7. T. R. Chay, Y. S. Lee and Y. S. Fan, *J. Theor. Biol.*, 1995, **174**, 21–44.
8. K. S. R. Cuthbertson and T. R. Chay, *Cell Calcium*, 1991, **12**, 97–109.
9. G. Dupont and C. Erneux, *Cell Calcium*, 1997, **22**, 321–331.
10. Y. X. Li and J. Rinzel, *J. Theor. Biol.*, 1994, **166**, 461–473.
11. A. Politi, L. D. Gaspers, A. P. Thomas and T. Hofer, *Biophys. J.*, 2006, **90**, 3120–3133.
12. J. Sneyd, Modeling IP3-dependent calcium dynamics in non-excitable cells, in *Tutorials in Mathematical Biosciences II*, Springer-Verlag, Berlin, 2005, Lecture Notes in Mathematics, vol. 1867, pp. 631–634.
13. L. Glass and M. C. Mackey, *J. Math. Biol.*, 1979, **7**, 339–352.

14. A. Jovic, B. Howell, M. Cote, S. M. Wade, K. Mehta, A. Miyawaki, R. R. Neubig, J. J. Linderman and S. Takayama, *PLoS Comput. Biol.*, 2010, **6**(12), e1001040.
15. R. Jacob, J. E. Merritt, T. J. Hallam and T. J. Rink, *Nature*, 1988, **335** 40–45.
16. M. Prentki, M. C. Glennon, A. P. Thomas, R. L. Morris, F. M. Matschinsky and B. E. Corkey, *J. Biol. Chem.*, 1988, **263**, 11044–11047.
17. N. M. Woods, K. S. Cuthbertson and P. H. Cobbold, *Nature*, 1986, **319**, 600–602.
18. M. S. Baptista and I. L. Caldas, *Nonlinear Dyn.*, 1998, **17**, 119–139.
19. M. R. Guevara, L. Glass and A. Shrier, *Science*, 1981, **214**, 1350–1353.
20. R. F. Galán and N. N. Urban, *Phys. Rev. Lett.*, 2005, **94**, 158101.
21. R. Wessel, *Eigenmannia*, *Biophys. J.*, 1995, **69**, 1880–1890.
22. S. Paliwal, C. J. Wang and A. Levchenko, *HFSP J.*, 2008, **2**, 251–256.
23. K. R. King, S. Wang, A. Jayaraman, M. L. Yarmush and M. Toner, *Lab Chip*, 2008, **8**, 107–116.
24. A. Sawano, S. Takayama, M. Matsuda and A. Miyawaki, *Dev. Cell*, 2002, **3**, 245–257.
25. S. Takayama, E. Ostuni, P. LeDuc, K. Naruse, D. E. Ingber and G. M. Whitesides, *Nature*, 2001, **411**, 1016–1016.
26. A. Jovic, B. Howell and S. Takayama, *Microfluid. Nanofluid.*, 2009, **6**, 717–729.
27. P. Hersen, M. N. McClean, L. Mahadevan and S. Ramanathan, *Proc. Natl. Acad. Sci. U. S. A.*, 2008, **105**, 7165–7170.
28. G. M. Whitesides, E. Ostuni, S. Takayama, X. Y. Jiang and D. E. Ingber, *Annu. Rev. Biomed. Eng.*, 2001, **3**, 335–373.
29. J. C. McDonald, D. C. Duffy, J. R. Anderson, D. T. Chiu, H. Wu, O. J. Schueller and G. M. Whitesides, *Electrophoresis*, 2000, **21**, 27–40.
30. J. N. Lee, X. Jiang, D. Ryan and G. M. Whitesides, *Langmuir*, 2004, **20**, 11684–11691.
31. G. Mehta, M. J. Kiel, J. W. Lee, N. Kotov, J. J. Linderman and S. Takayama, *Adv. Funct. Mater.*, 2007, **17**, 2701–2709.
32. M. A. Unger, H. P. Chou, T. Thorsen, A. Scherer and S. R. Quake, *Science*, 2000, **288**, 113–116.
33. N. Futai, W. Gu, J. W. Song and S. Takayama, *Lab Chip*, 2006, **6**, 149–154.
34. W. Gu, X. Y. Zhu, N. Futai, B. S. Cho and S. Takayama, *Proc. Natl. Acad. Sci. U. S. A.*, 2004, **101**, 15861–15866.
35. S. M. Langelier, D. S. Chang, R. I. Zeitoun and M. A. Burns, *Proc. Natl. Acad. Sci. U. S. A.*, 2009, **106**, 12617–12622.
36. B. Mosadegh, C. H. Kuo, Y. C. Tung, Y. S. Torisawa, T. Bersano-Begey, H. Tavana and S. Takayama, *Nat. Phys.*, 2010, **6**, 433–437.
37. A. Jovic, S. M. Wade, A. Miyawaki, R. R. Neubig, J. J. Linderman, *et al.*, Hi-fi transmission of periodic signals amid cell-to-cell variability. *Mol. BioSyst.*, 2011, in press, DOI: 10.1039/c1mb05031a.
38. A. Miyawaki, *Dev. Cell*, 2003, **4**, 295–305.

39. M. Akgoz, I. Azpiazu, V. Kalyanaraman and N. Gautam, *FASEB J.*, 2004, **18**, C257–C257.
40. A. Miyawaki, J. Llopis, R. Heim, J. M. McCaffery, J. A. Adams, M. Ikura and R. Y. Tsien, *Nature*, 1997, **388**, 882–887.
41. N. Mochizuki, S. Yamashita, K. Kurokawa, Y. Ohba, T. Nagai, A. Miyawaki and M. Matsuda, *Nature*, 2001, **411**, 1065–1068.
42. Y. Nino, K. Hotta and K. Oka. *PLoS ONE*, 2010, **5**(2), e9164.
43. V. Nikolaev, M. Bunemann, A. Hannawacker and M. J. Lohse, *Naunyn Schmiedebergs Arch. Pharmacol.*, 2004, **369**, R46–R46.
44. J. R. Blinks, W. G. Wier, P. Hess and F. G. Prendergast, *Prog. Biophys. Mol. Biol.*, 1982, **40**, 1–114.
45. G. Gryniewicz, M. Poenie and R. Y. Tsien, *J. Biol. Chem.*, 1985, **260**, 3440–3450.
46. K. R. Gee, K. A. Brown, W. N. U. Chen, J. Bishop-Stewart, D. Gray and I. Johnson, *Cell Calcium*, 2000, **27**, 97–106.
47. A. E. Palmer and R. Y. Tsien, *Nat. Protoc.*, 2006, **1**, 1057–1065.
48. T. Nagai, S. Yamada, T. Tominaga, M. Ichikawa and A. Miyawaki, *Proc. Natl. Acad. Sci. U. S. A.*, 2004, **101**, 10554–10559.
49. S. Marino, I. B. Hogue, C. J. Ray and D. E. Kirschner, *J. Theor. Biol.*, 2008, **254**, 178–196.
50. S. M. Blower and H. Dowlatabadi, *Int. Stat. Rev.*, 1994, **62**, 229–243.
51. J. Sneyd, K. Tsaneva-Atanasova, V. Reznikov, Y. Bai, M. J. Sanderson and D. I. Yule, *Proc. Natl. Acad. Sci. U. S. A.*, 2006, **103**, 1675–1680.
52. H. Shirakawa, M. Ito, M. Sato, Y. Umezawa and S. Miyazaki, *Biochem. Biophys. Res. Commun.*, 2006, **345**, 781–788.
53. J. Goedhart and T. W. J. Gadella, *J. R. Soc. Interface*, 2009, **6**, S27–S34.
54. X. Luo, S. Popov, A. K. Bera, T. M. Wilkie and S. Muallem, *Mol. Cell*, 2001, **7**, 651–660.
55. L. Chen, F. Azizi and C. H. Mastrangelo, *Lab Chip*, 2007, **7**, 850–855.
56. B. Kuczenski, W. C. Ruder, W. C. Messner and P. R. LeDuc, *PloS ONE*, 2009, **4**, 8.
57. J. Olofsson, H. Bridle, J. Sinclair, D. Granfeldt, E. Sahlin and O. Orwar, *Proc. Natl. Acad. Sci. U. S. A.*, 2005, **102**, 8097–8102.